Electronic Supplementary Material (ESI) for Journal of Materials Chemistry C.

Supporting information

Strong Nonlinear Optical Effect Attained by Atom-Response-Theory Aided Design in the $Na_2M^{II}M^{IV}_2Q_6$ (M^{II}=Zn, Cd; M^{IV}= Ge, Sn; Q= S, Se) Chalcogenide system

Run Ye,† Xiyue Cheng,† Bin-Wen Liu, Xiao-Ming Jiang,* Long-Qi Yang, Shuiquan Deng*, and Guo-Cong Guo*

CONTENTS

S1 Computational details

S1.1 VASP calculations.

The structural and electronic properties of the six $Na_2M^{II}M^{IV}{}_2Q_6$ (M^{II} = Zn, Cd; M^{IV} = Ge, Sn; Q = S, Se) type compounds were calculated within the framework of density functional theory (DFT) [1] by using the Vienna ab-initio simulation package (VASP) [2] with the projector augmented wave (PAW) method.[3] The generalized gradient approximation (GGA) within the Perdew-Burke-Ernzerhof (PBE) type exchange-correlation potentials [4] was used throughout this work. The employed PAW-PBE pseudopotentials [5] of elements Na, Zn, Cd, Ge, Sn, S and Se treat s^1p^6, $3d^{10}4s^2$, $4d^{10}5s^2$, $3d^{10}4s^24p^2$, $4d^{10}5s^25p^2$, $3s^23p^4$ and $4s^24p^4$ as the valence states, respectively. The plane wave cutoff energy for the expansion of wave functions was set at 500 eV and the tetrahedron method with Blöchl corrections was used for integrations in the first Brilloin Zone with dense *k*-point meshes, 8×8×8, 8×8×8, 8×8×8, 9×9×4, 8×8×4 and 7×7×4 for $Na_2ZnSn_2Se_6$ (NZSSe), $Na_2CdSn_2Se_6$ (NCSSe), $Na_2ZnSn_2S_6$ (NZSS), $Na_2ZnGe_2S_6$ (NZGS), $Na_2CdGe_2S_6$ (NCGS) and $Na_2CdGe_2Se_6$ (NCGSe), respectively. The quasi-Newton algorithm as implemented in the VASP code was used in all structural relaxations. In this work, both the cell volume and the atomic positions were all allowed to relax to minimize the internal forces. Excellent convergence of the energy differences (0.01 meV) and stress tensors (0.5 meV/Å) were achieved.
With the PBE-GGA[4] calculations, the band gaps (E_g) of the six $Na_2M^{II}M^{IV}{}_2Q_6$ compounds are calculated as presented in **Table S1**. The calculated E_g^{PBE} are remarkably smaller than the experimental values. In computing optical properties, this deficiency of the DFT is often corrected empirically by employing the scissor operation[6], in which the conduction bands are shifted in energy to have the experimental bandgap. In our calculations for the linear and nonlinear optical properties[7], we employed the SOS method[8] using the results obtained from the VASP optical module. The SOS formalism for second-order susceptibility was derived by Aversa and Sipe [8a] and later modified by Rashkeev *et al* [8b,8c] and Sharma *et. al*.[8d,8e] The calculated static dielectric constants, refractive indices *n* at 1910 nm and SHG tensors d_{ij} are shown in **Table S2 and S3**. Note that, the predicted SHG values of NZSSe and NCSSe shown in **Figure 1** were calculated based on the band gap, E_g^{HSE}, obtained by using the hybrid HSE06 functional [9] with mixing parameter α = 0.25.

S1.2 Partial response functional (PRF) method

The contribution of a certain occupied energy region between E_B and valence band maximum (VBM), $\zeta_V(E_B)$, to each SHG coefficient $\chi^{(2)}_{ijk}$ is determined by considering only those excitations from all occupied states between E_B and VBM to all the unoccupied states of the conduction bands (CBs), and the contribution, $\delta\zeta_V(E_B)$, of specific occupied states of energy E_B to each $\chi^{(2)}_{ijk}$ by the excitations from that energy to all unoccupied states of the CBs.

$$\delta\zeta_V(E_B) = -\frac{d\zeta_V(E_B)}{dE_B} \qquad (1)$$

Similarly, the contribution, $\zeta_C(E_B)$, of a certain unoccupied region between conduction band minimum (CBM) and E_B to each $\chi^{(2)}_{ijk}$ is determined by the excitations from all occupied states of the VBs only to all unoccupied states between CBM and E_B, and the contribution, $\delta\zeta_C(E_B)$, of specific unoccupied states of energy E_B to each $\chi^{(2)}_{ijk}$ by the excitations from all occupied states of the VBs only to that energy.

$$\delta\zeta_C(E_B) = \frac{d\zeta_C(E_B)}{dE_B} \quad (2)$$

S1.3 Atom response theory (ART) analysis

To evaluate the individual atom contributions to the SHG components, d_{ij}, it is computationally more convenient to express the corresponding PRFs in terms of the band index I_B, $\zeta(I_B)$,[7] where the band index I_B runs from 1 to N_{tot} (i.e., the total number of band orbitals) with increasing energy, E_B, from E_{min} to E_{max}. Here, $\zeta_V(I_B)$ and $\zeta_C(I_B)$ are denoted as ${}^{VB}\zeta_j$ and ${}^{CB}\zeta_j$, respectively, with I_B replaced by a subscript j.

Suppose that a specific atom τ has L atomic orbitals with a coefficient ${}^{VB}C_{L\tau}^{\vec{k}j}$ in the valence band j at a wave vector $\vec{k}$. The total contribution ${}^{VB}A_\tau$ of an atom τ makes to the SHG coefficient from all the VB bands j is written as

$${}^{VB}A_\tau = \frac{\Omega}{(2\pi)^3}\int d\vec{k} \cdot \sum_{L,j} {}^{VB}\zeta_j \left|{}^{VB}C_{L\tau}^{\vec{k}j}\right|^2 \quad (3)$$

where Ω is the unit cell volume, ${}^{VB}\zeta_j$ is the corresponding PRFs in terms of the band index j. Similarly, the total contribution ${}^{CB}A_\tau$ of an atom τ makes to the SHG coefficient from all the CB bands j is written as

$${}^{CB}A_\tau = \frac{\Omega}{(2\pi)^3}\int d\vec{k} \cdot \sum_{L,j} {}^{CB}\zeta_j \left|{}^{CB}C_{L\tau}^{\vec{k}j}\right|^2 \quad (4)$$

in which we assumed that the atom has L atomic orbitals with coefficient ${}^{CB}C_{L\tau}^{\vec{k}j}$ in the conduction band j at a wave vector $\vec{k}$. To calculate the actual contribution of each constituent atom in a unit cell to the total SHG response, one needs to consider the signs of ${}^{VB}\zeta_j$ and ${}^{CB}\zeta_j$.

The total contribution, A_τ, each individual atom makes to the SHG response from both the VBs and the CBs (i.e., from all the bands) is given by

$$A_\tau = \frac{\left({}^{VB}A_\tau + {}^{CB}A_\tau\right)}{2} \quad (5)$$

where the factor of 1/2 is applied to remove the double counting of each excitation.

S2 Experimental section

S2.1 Synthesis

The following chemicals were used in this work: Na (99.7%), Zn (99.99%), Cd (99.99%), Sn (99.9%), and Se (99.9%). All of these chemicals were bought from Aladdin Chemistry Co. Ltd and used without further purification. The starting material Na_2Se was prepared through the stoichiometric reaction of Na and Se in liquid ammonia. For the synthesis of the target compounds, a mixture of the starting materials Na_2Se, Zn for **1** or Cd for **2**, Sn and Se in a molar ratio of 1: 1: 2: 6, were loaded into a graphite crucible and placed in quartz tubes. The tubes were flame-sealed under vacuum (~10^{-4} Torr) and then placed in a muffle furnace, heated

from room temperature to 875K in 40 hours, kept at that temperature for 96 hours, and then cooled to room temperature with a rate of 4 K/hour. The products were washed with water and dried with ethanol. The pure red crystals of **1** and **2** were manually picked out. The yields were about 75% for **1** and 65% for **2** based on Zn/Cd, respectively.

S2.2 Single-crystal structure determination

The measurements of single crystals of **1** and **2** were performed on a Pilatus CCD diffractometer equipped with graphite-monochromated Mo−Kα radiation (λ = 0.71073 Å) at 293 K. A ω-scan technique was used for the collection of intensity data sets, and the data sets were reduced using CrystalClear. The structures of **1** and **2** were solved by ShelXT structure solution program and refined through full-matrix least-square technique on F^2. All of the calculations were performed using Olex2. The final structures were examined for additional symmetry with ADDSYM/PLATON and no other missed or higher symmetry was observed. The crystallographic data and structural refinement information for **1** and **2** are given in **Table S5**. Atomic coordinates and the selected bond distances are listed in **Tables S6** and **S7**, respectively. Semiquantitative microprobe element analyses of crystals of **1** and **2** were performed with a field emission scanning electron microscope (FESEM, JSM6700F) equipped with an energy-dispersive X-ray spectroscopy instrument (EDX, Oxford INCA). The obtained empirical formulas $Na_{3.0}Zn_{0.9}Sn_{2.0}Se_{6.0}$ of **1** and $Na_{1.9}Cd_{1.0}Sn_{1.7}Se_{6.0}$ of **2** were consistent with the results determined from single-crystal XRD. Further details of the crystal structure investigations may be obtained from the Fachinformationszentrum Karlsruhe, 76344 Eggenstein-Leopoldshafen (Germany), on quoting the depository number CSD-1955642 and -1955644, for **1** and **2**, respectively.

S2.3 Powder X-ray diffraction

The powder XRD patterns were recorded on a Rigaku MiniFlex 600 diffractometer using Cu Kα radiation (λ = 1.5406 Å) in the reflection mode at room temperature with a step width of 0.02°. Both the experimental and simulated PXRD patterns of **1** and **2** are presented in Figure S1. No impurity peak was observed in the experimental patterns of both compounds.

S2.4 UV−Vis−NIR diffuse reflectance and infrared spectroscopy

The UV−vis diffuse reflectance spectra of powder samples of 1 and 2 were recorded at room temperature on a PerkinElmer Lambda 900 UV−vis spectrometer in the range of 200 nm to 2000 nm with BaSO4 as the reference. The absorption spectra were obtained from the diffuse reflectance spectra by using the Kubelka−Munk function: α/S = (1−R)2/2R, where α is the absorption coefficient, S is the scattering coefficient, and R is the reflectance.

The IR spectra of 1 and 2 were obtained using a PerkinElmer Spectrum One FR-IR Spectrometer in the range of 400 cm-1 to 4000 cm-1 at room temperature. The powder samples of 1 and 2 were diluted with dry KBr and pressed into transparent pellets for the measurement.

S2.5 SHG measurements

SHG measurements of **1** and **2** were performed by using a modified Kurtz−Perry powder technique with a 1910 nm laser radiation. The powder samples were ground and sieved into five distinct particle size ranges of 30-50, 50-100, 100-150, 150-200 and 200-250 μm for the SHG phase-matchable measurements. The AGS crystals with the same particle size ranges served as the standard. The doubled frequency signals (955 nm) were detected by an Andor DU420A-BR-DD CCD camera after the mixed signals passed through the monochromator.

S2.6 Powder LIDTs Measurements

The single pulse measurement method was used to estimate the powder LIDTs. The samples of **1** and **2** and the reference AGS in the same size range of 50-100 μm were pressed into glass microscope cover slides. The samples were subjected to high-power 1064 nm laser radiation with pulse width τ_p of 10 ns in a 1 Hz repetition. An optical concave lens was used to adjust the diameter of the laser to obtain different intensities. The investigations were carried out by gradually increasing the laser power until the color of the sample changed, which is chosen as the critical point to estimate the damage threshold. The damage threshold was derived from the equation $I_{threshold} = E/(\pi r^2 t)$, where E is the energy of a single pulse, r is the spot radius, and t is pulse width.

S3. Tables

Table S1. Optimized lattice parememters in standard setting, *a* (Å), *b* (Å), *c* (Å), and β (°), the relaxed primitive cell volme *V* (Å^3), calculated energy gap E_g^{PBE} (eV), experimental gap E_g^{Exp} (eV) and the cell volume to bandgap ratio V/E_g^{Exp} for $Na_2ZnSn_2Se_6$ (NZSSe, **1**), $Na_2CdSn_2Se_6$ (NCSSe, **2**), $Na_2ZnSn_2S_6$ (NZSS), $Na_2ZnGe_2S_6$ (NZGS), $Na_2CdGe_2S_6$ (NCGS) and $Na_2CdGe_2Se_6$ (NCGSe).

Chemical Formula	$Na_2ZnSn_2Se_6$[a]	$Na_2CdSn_2Se_6$[a]	$Na_2ZnSn_2S_6$[b]	$Na_2ZnGe_2S_6$[c]	$Na_2CdGe_2S_6$[d]	$Na_2CdGe_2Se_6$[d]
	NZSSe (**1**)	NCSSe (**2**)	NZSS	NZGS	NCGS	NCGSe
Space group	*Fdd*2	*Fdd*2	*Fdd*2	*Cc*	*Cc*	*Cc*
Point group	*mm*2	*mm*2	*mm*2	*m*	*m*	*m*
Lattice parameters (Å)	*a* = 13.745	*a* = 13.819	*a* = 13.148	*a* = 7.433	*a* = 7.467	*a* = 7.792
	b = 25.097	*b* = 25.756	*b* = 24.012	*b* = 12.555	*b* = 12.812	*b* = 13.422
	c = 7.725	*c* = 7.810	*c* = 7.414	*c* = 11.762	*c* = 11.782	*c* = 12.384
				β = 102.462°	β = 99.029°	β = 99.037°
V (Å^3)	666.22	694.89	585.20	535.87	556.57	640.03
E_g^{PBE} (eV)	1.099	1.045	1.704	2.234	2.219	1.382
E_g^{HSE} (eV)	1.972	1.911				
E_g^{Exp} (eV)	2.05 [a]	2.15 [a]	2.71 [b]	3.25 [c]	3.21 [d]	2.37 [d]
V/E_g^{Exp} (Å^3/eV)	324.98	323.20	215.94	164.88	173.39	270.05

[a] This work.

[b] Ref. [10].

[c] Ref. [11].

[d] Ref. [12].

Table S2. Calculated static dielectric constants and refractive indices *n* at 1910 nm along the three main directions [100], [010] and [001], as well as the calculated birefringence Δ*n* (at 1910 nm) for NZSSe (**1**), NCSSe (**2**), NZSS, NZGS, NCGS and NCGSe. The only available reported reference data of NZGS is also listed for comparison.

Compounds	ε (*xx*)	ε (*yy*)	ε (*zz*)	*n* (*xx*)	*n* (*yy*)	*n* (*zz*)	Δ*n*	Reported Δ*n*
NZSSe (1)	6.131	5.884	5.787	2.499	2.444	2.424	0.075	
NCSSe (2)	5.787	5.595	5.622	2.425	2.381	2.388	0.044	
NZSS	4.914	4.886	4.780	2.228	2.221	2.196	0.031	
NZGS	4.719	4.831	4.775	2.181	2.207	2.194	0.026	0.026[a]
NCGS	4.739	4.821	4.767	2.186	2.205	2.193	0.019	
NCGSe	5.681	5.807	5.693	2.399	2.426	2.402	0.027	

[a] Calculated Δ*n* at 1.06 μm. [11]

Table S3. Calculated SHG tensors d_{ij} and d_{eff} at 0 eV and 1910 nm for NZSSe (**1**), NCSSe (**2**), NZSS, NZGS, NCGS and NCGSe. For NZSSe (**1**), NCSSe (**2**) and NZSS with the point group *mm*2, there are five nonzero nonlinear coefficients, d_{31}, d_{32}, d_{33}, d_{15} and d_{24}, while for NZGS, NCGS and NCGSe with the point group *m*, there are ten nonzero nonlinear coefficients, d_{11}, d_{12}, d_{13}, d_{15}, d_{24}, d_{26}, d_{31}, d_{32}, d_{33} and d_{35}. During our calculation, the Kleinman symmetry was not assumed. The experimental SHG intensity and the estimated $d_{\mathrm{eff}}^{\mathrm{Exp}}$ are also presented for comparison.

	NZSSe (**1**)	NCSSe (**2**)	NZSS	NZGS	NCGS	NCGSe
d_{ij} (ω = 0)	d_{31} = 23.607 d_{32} = -13.938 d_{33} = 15.287 d_{15} = 13.789 d_{24} = -12.525	d_{31} = 18.684 d_{32} = -13.410 d_{33} = 14.853 d_{15} = 10.256 d_{24} = -10.913	d_{31} = 6.205 d_{32} = -8.789 d_{33} = 5.964 d_{15} = 5.608 d_{24} = -7.957	d_{11} = -5.909 d_{12} = -5.467 d_{13} = 3.587 d_{15} = 2.062 d_{24} = 1.185 d_{26} = -5.427 d_{31} = 1.542 d_{32} = 0.989 d_{33} = -0.550 d_{35} = 3.707	d_{11} = -5.442 d_{12} = -5.080 d_{13} = 3.983 d_{15} = 4.092 d_{24} = 1.116 d_{26} = -5.381 d_{31} = 3.701 d_{32} = 1.071 d_{33} = -2.633 d_{35} = 4.061	d_{11} = 8.104 d_{12} = 11.900 d_{13} = -6.809 d_{15} = -7.464 d_{24} = -1.443 d_{26} = 9.487 d_{31} = -5.903 d_{32} = -1.903 d_{33} = 2.439 d_{35} = -7.454
d_{eff} (ω = 0)	12.07	10.07	5.66	4.86	5.31	9.21
d_{ij} (ω = 1910 nm)	d_{32} = -24.845 d_{33} = 28.575 d_{31} = 46.826 d_{15} = 27.842 d_{24} = -21.124	d_{31} = 34.249 d_{32} = -23.364 d_{33} = 26.732 d_{15} = 18.968 d_{24} = -17.925	d_{31} = 10.563 d_{32} = -13.822 d_{33} = 9.501 d_{15} = 9.138 d_{24} = -12.191	d_{11} = -8.808 d_{12} = -8.354 d_{13} = 5.141 d_{15} = 3.029 d_{24} = 1.723 d_{26} = -8.126 d_{31} = 2.290 d_{32} = 1.468 d_{33} = -0.397 d_{35} = 5.260	d_{11} = -8.130 d_{12} = -7.670 d_{13} = 5.757 d_{15} = 6.154 d_{24} = 1.641 d_{26} = -7.928 d_{31} = 5.638 d_{32} = 1.646 d_{33} = -3.584 d_{35} = 5.835	d_{11} = 13.233 d_{12} = 20.533 d_{13} = -10.957 d_{15} = -12.760 d_{24} = -2.643 d_{26} = 15.569 d_{31} = -10.651 d_{32} = -3.633 d_{33} = 2.356 d_{35} = -12.081
d_{eff} (ω = 1910 nm)	23.45	18.17	8.84	7.22	7.86	15.35
Exp. SHG	3×AGS [a]	2.2×AGS [a]	4×AGS [b]	0.9×AGS [c]	0.8×AGS [d]	2×AGS [d]
d_{eff}^{Exp} [e]	23.73	20.32	27.40	13.00	12.25	19.37
Other work			maximum d_{ij} 7.4 [g]	d_{11} = -4.3 [f] d_{12} = 4.63 [f] d_{13} = -5.3 [f] d_{15} = -4.3 [f] d_{24} = 4.63 [f] d_{33} = -5.3 [f]		

[a] This work. Powder SHG intensity at ω = 1910 nm.

[b] Powder SHG intensity at ω = 2.09 nm. [10]

[c] Powder SHG intensity at ω = 2.09 nm. [11]

[d] Powder SHG intensity at ω = 2.09 nm. [12]

[e] Estimated from experimental powder SHG data in this work. As the measured intensity of the SHG signal by using the Kurtz−Perry powder method is proportional to the square of effective SHG coefficient d_{eff}. d_{eff}^{Exp} is

estimated by $d_{eff}^{Exp} = (N \times d_{eff}^{AGS2})^{1/2}$, where *N* is the measured multiple comparing with the SHG signal intensity of AGS, d_{eff}^{AGS} is 13.7 pm/V at 1910 nm.

[f] Static d_{ij} by the DFT methods. [11]

[g] Static SHG tensor by the DFT methods. [12]

Table S4. Contributions of the individual atoms to the strongest SHG coefficient. (a) d_{31} of $Na_2ZnSn_2Se_6$ (NZSSe), (b) d_{31} of $Na_2CdSn_2Se_6$ (NCSSe), (c) d_{32} of $Na_2ZnSn_2S_6$ (NZSS), (d) d_{11} of $Na_2ZnGe_2S_6$ (NZGS), (e) d_{11} of $Na_2CdGe_2S_6$ (NCGS) and (f) d_{12} of $Na_2CdGe_2Se_6$ (NCGSe). W_A refers to the number of the same type of atoms (on the same Wyckoff site) in a unit cell. A_τ is the contribution (in %) from a single atom τ, and C_A from all atoms of the same type. ${}^{VB}A_\tau$, is the contribution (in %) the VBs, and ${}^{CB}A_\tau$ from the CBs. The contributions from the *s*, *p* and *d* states of the atom τ to ${}^{VB}A_\tau$ and ${}^{CB}A_\tau$ are also shown.

(a) NZSSe-d_{31}

Atom	W_A	A_τ	C_A	${}^{VB}A_\tau$	${}^{CB}A_\tau$	${}^{VB}_{s}A_\tau$	${}^{VB}_{p}A_\tau$	${}^{VB}_{d}A_\tau$	${}^{CB}_{s}A_\tau$	${}^{CB}_{p}A_\tau$	${}^{CB}_{d}A_\tau$
Na	4	0.66	2.63	0.19	0.46	0.04	0.16	0.00	0.34	0.12	0.00
Zn	2	2.41	4.83	0.93	1.48	-0.28	0.49	0.72	0.67	0.67	0.14
Sn	4	5.92	23.69	2.31	3.61	0.78	1.21	0.32	0.84	2.45	0.32
Se1	4	6.16	24.63	4.74	1.42	-0.02	4.75	0.00	0.22	1.04	0.17
Se2	4	5.88	23.51	4.40	1.48	-0.01	4.40	0.00	0.19	1.13	0.16
Se3	4	5.18	20.70	3.25	1.92	-0.40	3.65	0.01	0.21	1.51	0.21

(b) NCSSe-d_{31}

Atom	W_A	A_τ	C_A	${}^{VB}A_\tau$	${}^{CB}A_\tau$	${}^{VB}_{s}A_\tau$	${}^{VB}_{p}A_\tau$	${}^{VB}_{d}A_\tau$	${}^{CB}_{s}A_\tau$	${}^{CB}_{p}A_\tau$	${}^{CB}_{d}A_\tau$
Na	4	0.75	3.02	0.23	0.52	0.04	0.19	0.00	0.39	0.14	0.00
Cd	2	1.00	2.00	-0.63	1.63	-0.17	0.46	-0.93	0.59	0.90	0.14
Sn	4	6.14	24.56	2.49	3.65	0.99	1.10	0.39	0.36	2.92	0.38
Se1	4	5.88	23.51	4.57	1.31	-0.12	4.69	0.00	0.17	0.97	0.18
Se2	4	6.39	25.56	5.06	1.33	-0.12	5.18	0.00	0.21	0.94	0.18
Se3	4	5.34	21.35	3.51	1.83	-0.30	3.79	0.01	0.28	1.33	0.22

(c) NZSS-d_{32}

Atom	W_A	A_τ	C_A	${}^{VB}A_\tau$	${}^{CB}A_\tau$	${}^{VB}_{s}A_\tau$	${}^{VB}_{p}A_\tau$	${}^{VB}_{d}A_\tau$	${}^{CB}_{s}A_\tau$	${}^{CB}_{p}A_\tau$	${}^{CB}_{d}A_\tau$
Na	4	1.97	7.89	0.24	1.73	0.05	0.19	0.00	1.24	0.50	0.00
Zn	2	3.82	7.64	0.32	3.50	0.48	0.71	-0.88	0.69	2.42	0.39
Sn	4	3.12	12.47	0.01	3.10	0.24	0.50	-0.73	-1.45	3.66	0.90
S1	4	7.77	31.09	6.11	1.67	-0.08	6.19	0.00	0.19	1.48	0.00
S2	4	6.86	27.44	5.71	1.15	-0.07	5.78	0.00	0.07	1.08	0.00
S3	4	3.37	13.48	3.06	0.31	-0.24	3.30	0.00	-0.02	0.33	0.00

(d) NZGS-d_{11}

Atom	W_A	A_τ	C_A	${}^{VB}A_\tau$	${}^{CB}A_\tau$	${}^{VB}_{s}A_\tau$	${}^{VB}_{p}A_\tau$	${}^{VB}_{d}A_\tau$	${}^{CB}_{s}A_\tau$	${}^{CB}_{p}A_\tau$	${}^{CB}_{d}A_\tau$
Na1	2	0.99	1.98	0.18	0.82	0.06	0.12	0.00	0.35	0.47	0.00
Na2	2	0.73	1.46	-0.04	0.77	0.04	-0.08	0.00	0.30	0.47	0.00
Zn	2	3.39	6.79	1.31	2.09	0.78	0.71	-0.19	0.55	1.13	0.40
Ge1	2	4.66	9.32	1.79	2.87	0.02	1.50	0.27	0.78	1.34	0.75
Ge2	2	4.88	9.77	1.93	2.96	0.05	1.51	0.36	0.83	1.37	0.75
S1	2	6.56	13.13	5.38	1.19	-0.20	5.57	0.00	0.18	1.01	0.00
S2	2	6.21	12.43	4.96	1.25	-0.33	5.30	0.00	0.18	1.07	0.00
S3	2	6.65	13.29	5.38	1.27	-0.32	5.70	0.00	0.18	1.08	0.00
S4	2	4.96	9.92	3.48	1.48	-0.35	3.83	0.00	0.20	1.28	0.00
S5	2	5.92	11.84	4.70	1.22	-0.32	5.02	0.00	0.16	1.06	0.00
S6	2	5.03	10.07	3.69	1.34	-0.34	4.02	0.00	0.16	1.18	0.00

(e)NCGS-d_{11}

Atom	W_A	A_τ	C_A	${}^{VB}A_\tau$	${}^{CB}A_\tau$	${}^{VB}_{s}A_\tau$	${}^{VB}_{p}A_\tau$	${}^{VB}_{d}A_\tau$	${}^{CB}_{s}A_\tau$	${}^{CB}_{p}A_\tau$	${}^{CB}_{d}A_\tau$
Na1	2	1.00	2.00	0.10	0.90	0.05	0.05	0.00	0.38	0.52	0.00
Na2	2	0.69	1.38	-0.21	0.90	0.03	-0.24	0.00	0.35	0.55	0.00
Cd	2	0.72	1.44	-1.20	1.92	0.61	0.59	-2.40	0.35	1.18	0.39
Ge1	2	5.01	10.02	2.14	2.87	0.09	1.47	0.59	0.67	1.39	0.81
Ge2	2	4.12	8.25	1.63	2.49	0.07	1.45	0.11	0.33	1.34	0.81
S1	2	7.12	14.24	6.08	1.04	-0.45	6.53	0.00	0.13	0.91	0.00
S2	2	5.14	10.29	3.92	1.22	-0.14	4.06	0.00	0.15	1.06	0.00
S3	2	7.45	14.90	6.43	1.02	-0.43	6.86	0.00	0.12	0.90	0.00
S4	2	5.36	10.72	4.13	1.23	-0.19	4.32	0.00	0.16	1.07	0.00
S5	2	6.40	12.80	5.18	1.23	-0.32	5.50	0.00	0.15	1.07	0.00
S6	2	6.98	13.96	5.90	1.08	-0.16	6.05	0.00	0.14	0.94	0.00

(f) NCGSe-d_{12}

Atom	W_A	A_τ	C_A	${}^{VB}A_\tau$	${}^{CB}A_\tau$	${}^{VB}_{s}A_\tau$	${}^{VB}_{p}A_\tau$	${}^{VB}_{d}A_\tau$	${}^{CB}_{s}A_\tau$	${}^{CB}_{p}A_\tau$	${}^{CB}_{d}A_\tau$
Na1	2	0.81	1.61	0.19	0.62	0.05	0.14	0.00	0.47	0.15	0.00
Na2	2	0.99	1.99	0.31	0.68	0.04	0.27	0.00	0.51	0.17	0.00
Cd	2	3.33	6.66	1.68	1.65	0.38	0.45	0.85	0.60	0.87	0.18
Ge1	2	5.69	11.38	1.22	4.47	0.04	1.38	-0.21	1.48	2.64	0.36
Ge2	2	5.51	11.01	1.43	4.07	-0.02	1.06	0.40	1.52	2.22	0.34
Se1	2	4.12	8.24	2.20	1.92	0.57	1.63	0.00	0.17	1.53	0.23
Se2	2	3.94	7.88	1.76	2.18	0.03	1.72	0.01	0.23	1.68	0.27
Se3	2	6.48	12.96	4.45	2.03	0.13	4.32	0.01	0.19	1.59	0.25
Se4	2	6.81	13.63	3.93	2.88	-0.01	3.93	0.01	0.26	2.26	0.37
Se5	2	6.32	12.64	4.21	2.11	0.40	3.81	0.00	0.25	1.60	0.26
Se6	2	6.00	12.00	3.24	2.76	0.04	3.19	0.01	0.28	2.12	0.36

Table S5. Experimental crystallographic data and structural refinement information for **1** and **2**.

	$Na_2ZnSn_2Se_6$ (**1**)	$Na_2CdSn_2Se_6$ (**2**)
Temperature (K)	293	
Space group	*Fdd2*	
a (Å)	24.6051(7)	25.1984(14)
b (Å)	13.5164(4)	13.4933(9)
c (Å)	7.6031(2)	7.6733(5)
V (Å^3)	2528.58(12)	2609.0(3)
Z	8	8
D_{calcd} (g cm^{-3})	4.321	4.427
μ (mm^{-1})	23.087	22.167
ϑ range (deg)	7.906 - 62.502	7.802 - 53.99
GOF on F^2	1.089	1.100
R_1[a] [$I > 2\sigma(I)$]	0.0156	0.0229
wR_2[b] [$I > 2\sigma(I)$]	0.0357	0.0548
R_1[a] (all data)	0.0161	0.0236
wR_2[b] (all data)	0.0358	0.0550
Flack parameter *x*	0.012(4)	0.003(10)
$\Delta\rho_{max}/\Delta\rho_{min}$(eÅ^{-3})	0.68/-0.86	0.80/-0.65

[a] $R_1 = \Sigma||F_o| - |F_c||/\Sigma|F_o|$;

[b] $wR_2 = \Sigma[(w(F_o^2 - F_c^2)^2)/\Sigma[w(F_o^2)^2)]^{1/2}$

Table S6. Atomic coordinates and equivalent isotropic displacement parameters of **1** and **2**. U_{eq} is defined as 1/3 of the trace of the orthogonalized U_{IJ} tensor.

Compounds	Atom	*x*	*y*	*z*	U_{eq}(Å^2)
1	Sn(1)	0.6391(2)	0.3754(2)	0.5234(4)	0.014(7)
	Se(1)	0.5140(2)	0.6490(3)	0.6856(6)	0.021(10)
	Se(2)	0.5796(2)	0.4679(3)	0.3142(6)	0.019(9)
	Se(3)	0.6130(2)	0.1964(3)	0.5877(6)	0.018(9)
	Zn(1)	0.5000	0.5000	0.5031(10)	0.018(14)
	Na(1)	0.6413(2)	0.8323(2)	0.5159(4)	0.053(7)
2	Sn(1)	0.6413(2)	0.3839(4)	0.6003(7)	0.017(18)
	Cd(1)	0.5000	0.5000	0.5782(13)	0.023(2)
	Se(1)	0.5846(3)	0.4712(7)	0.3831(10)	0.022(2)
	Se(2)	0.7364(3)	0.4096(7)	0.5225(13)	0.024(3)
	Se(3)	0.6156(4)	0.2045(6)	0.6603(12)	0.020(2)
	Na(1)	0.6989(19)	0.5844(4)	0.3393(6)	0.050(12)

Table S7. Selected bond lengths (Å) in **1** and **2**.

1			
Sn(1)-Se(1)#1	2.4960(5)	Se(2)-Na(1)#4	3.020(3)
Sn(1)-Se(2)	2.4969(5)	Se(3)-Sn(1)#1	2.5760(5)
Sn(1)-Se(3)#2	2.5760(5)	Se(3)-Na(1)#5	3.010(3)
Sn(1)-Se(3)	2.5498(5)	Zn(1)-Se(1)#6	2.4694(6)
Sn(1)-Na(1)#1	3.753(3)	Zn(1)-Se(2)#6	2.4674(6)
Se(1)-Sn(1)#2	2.4960(5)	Na(1)-Sn(1)#2	3.753(3)
Se(1)-Zn(1)	2.4695(6)	Na(1)-Se(1)#7	2.944(3)
Se(1)-Na(1)	2.913(3)	Na(1)-Se(2)#8	3.020(3)
Se(1)-Na(1)#3	2.944(3)	Na(1)-Se(2)#2	3.415(3)
Se(2)-Zn(1)	2.4674(6)	Na(1)-Se(3)#9	3.010(3)
Se(2)-Na(1)#1	3.415(3)		
Symmetry transformations used to generate equivalent atoms: *#1 5/4-X,-1/4+Y,-1/4+Z; #2 5/4-X,1/4+Y,1/4+Z; #3 1-X,3/2-Y,1/2+Z;* *#4 +X,-1/2+Y,-1/2+Z; #5 5/4-X,-3/4+Y,1/4+Z; #6 1-X,1-Y,+Z;* *#7 1-X,3/2-Y,-1/2+Z; #8 +X,1/2+Y,1/2+Z; #9 5/4-X,3/4+Y,-1/4+Z*			
2			
Sn(1)-Se(1)	2.4904(10)	Se(1)-Na(1)#4	3.034(5)
Sn(1)-Se(2)	2.4951(10)	Se(2)-Cd(1)#5	2.6414(11)
Sn(1)-Se(3)	2.5479(10)	Se(2)-Na(1)#6	2.928(5)
Sn(1)-Se(3)#1	2.5687(11)	Se(2)-Na(1)	2.904(5)
Sn(1)-Na(1)	3.666(5)	Se(3)-Sn(1)#4	2.5687(11)
Cd(1)-Se(1)#2	2.6341(10)	Se(3)-Na(1)#7	2.986(5)
Cd(1)-Se(1)	2.6341(10)	Na(1)-Se(1)#1	3.034(5)
Cd(1)-Se(2)#3	2.6414(11)	Na(1)-Se(2)#8	2.928(5)
Cd(1)-Se(2)#1	2.6414(11)	Na(1)-Se(3)#9	2.986(5)
Se(1)-Na(1)	3.276(5)		
Symmetry transformations used to generate equivalent atoms: *#1 5/4-X,-1/4+Y,-1/4+Z; #2 1-X,1-Y,+Z; #3 -1/4+X,3/4-Y,1/4+Z;* *#4 5/4-X,-1/4+Y,-1/4+Z; #5 1/4+X,3/4-Y,-1/4+Z; #6 3/2-X,1-Y,1/2+Z;* *#7 +X,-1/2+Y,1/2+Z; #8 3/2-X,1-Y,-1/2+Z; #9 +X,1/2+Y,-1/2+Z*			

S4. Figures

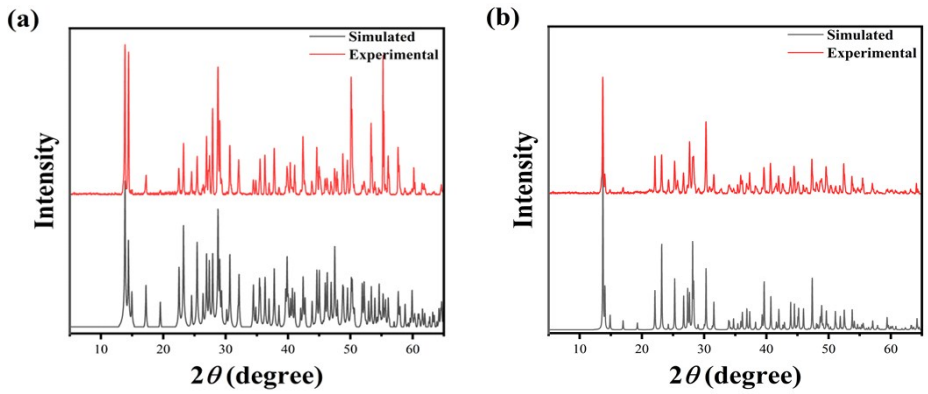

Figure S1. Experimental and simulated powder X-ray diffraction patterns of **1** (a) and **2** (b).

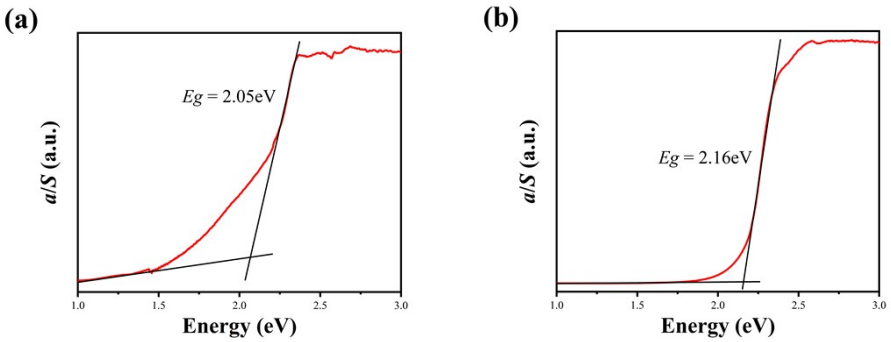

Figure S2. UV – Vis diffuse reflectance spectra of **1** (a) and **2** (b).

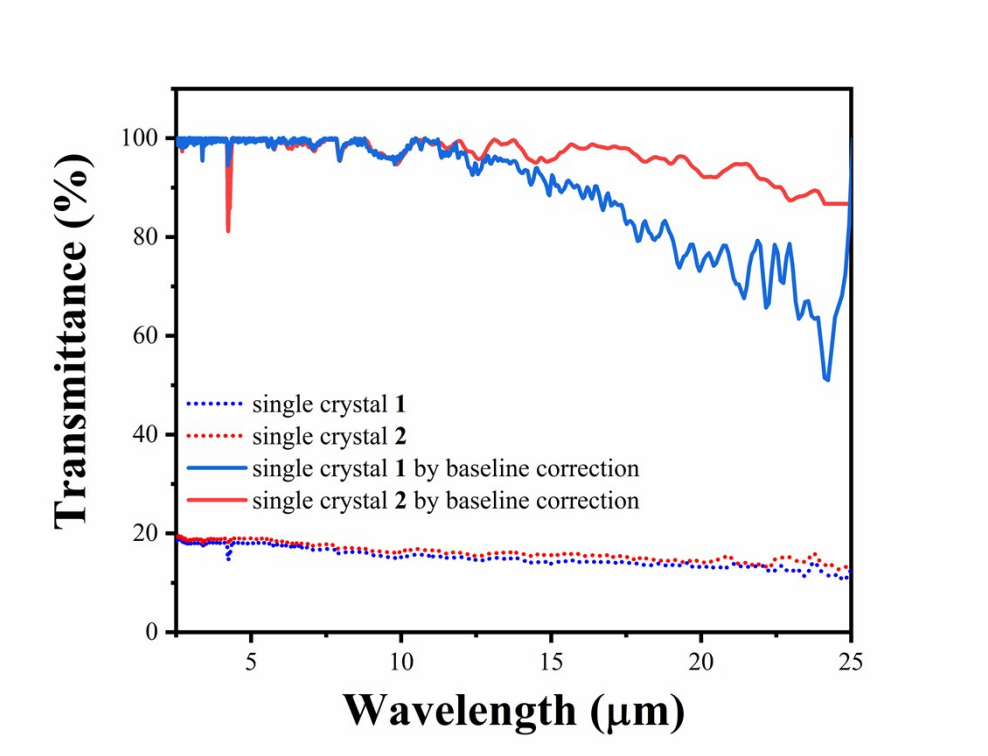

Figure S3. Single crystal IR spectra of **1** and **2**.

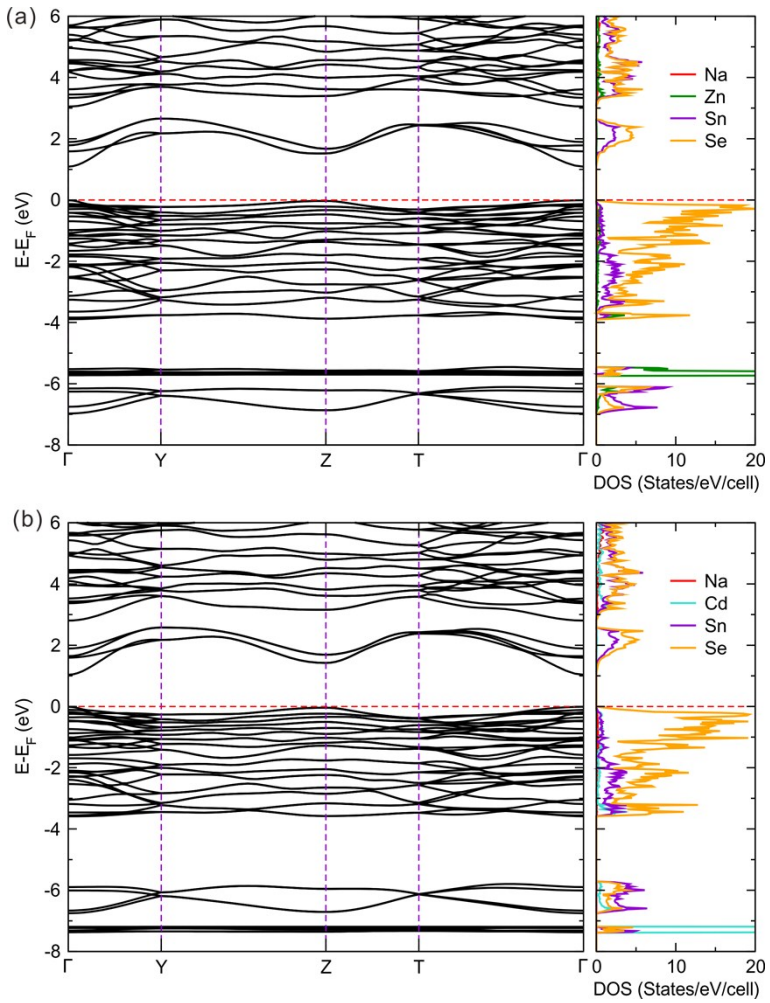

Figure S4. Calculated band structures and total density of states (TDOS) of **1** (a) and **2** (b). The Fermi level is set at 0 eV. The direct band gaps of **1** and **2** are calculated as 1.099 and 1.045 eV, respectively.

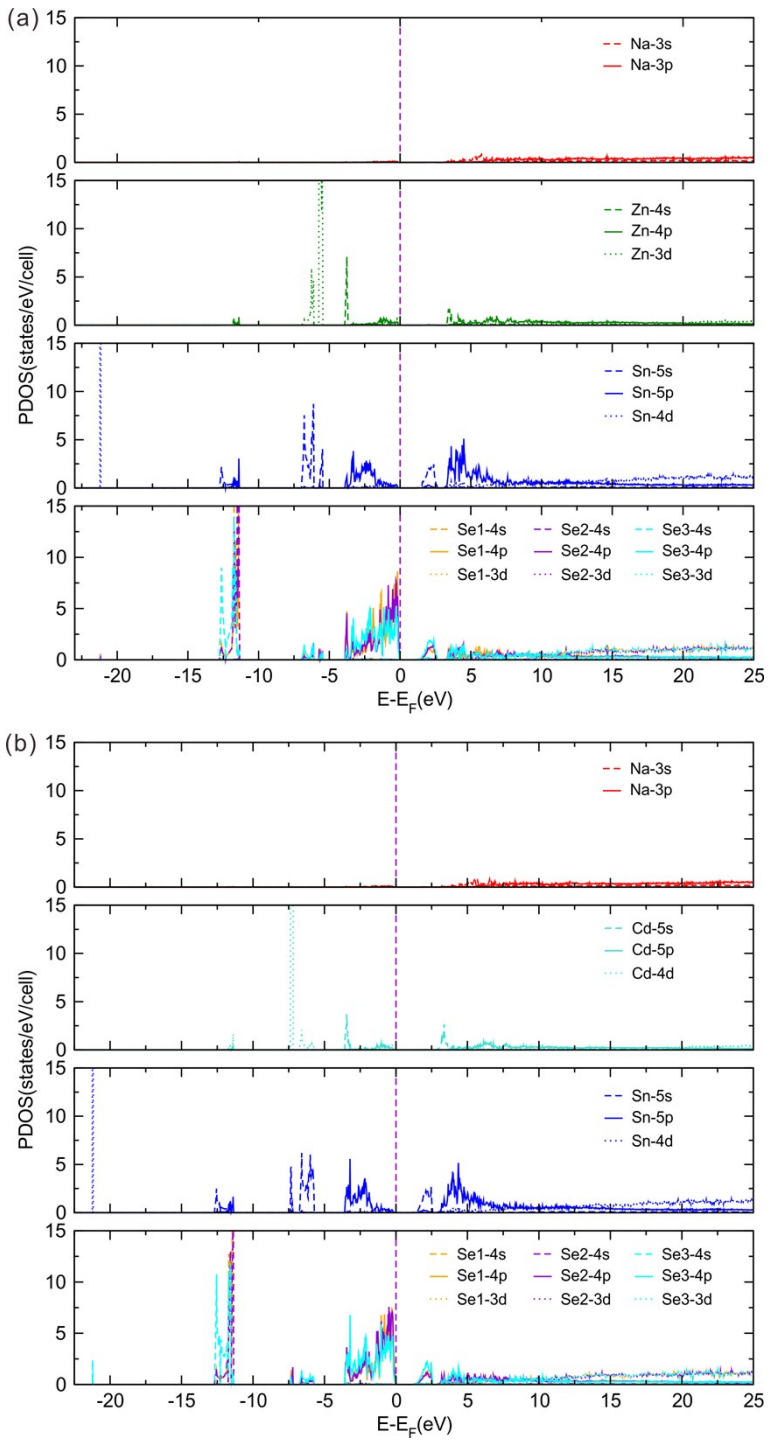

Figure S5. Partial density of states (PDOS) plots of **1** (a) and **2** (b). The top valence bands (-2 eV to the Fermi level) are mainly composed of Se-4p states, whereas hybridized Sn-5p orbitals and Se-4p states are found from -4 to -2 eV, together with small amount of Zn-4s states in **1** (Cd-5s states in **2**). The bottom of the conduction bands (E_g-2.8 eV) are primarily composed of Se-4p and Sn-5s states, while the mixture of Sn-p, Zn-4s/p (Cd-5s/p) and Se-4s/p orbitals occur in the higher energy range from 2.8 to 8 eV.

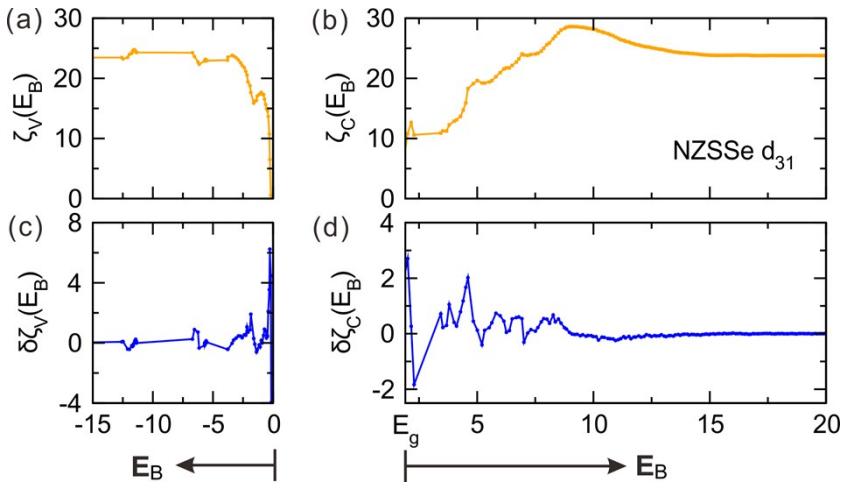

Figure S6. (a) $\zeta_V(E_B)$-vs-E_B plot, (b) $\zeta_C(E_B)$-vs-E_B plot, (c) $\delta\zeta_V(E_B)$-vs-E_B plot, and (d) $\delta\zeta_C(E_B)$-vs-E_B plot calculated for the SHG coefficient d_{31} of NZSSe (**1**). The values of the functions are in pm/V. The PRF functionals are described in S1.2.

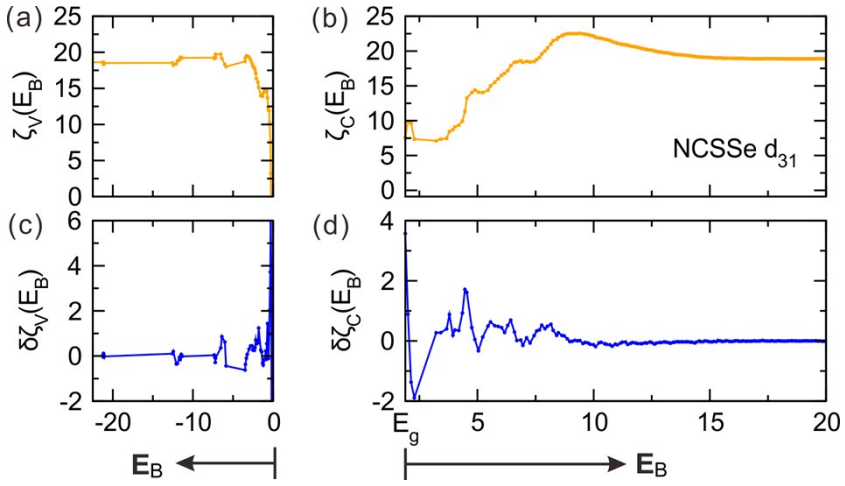

Figure S7. (a) $\zeta_V(E_B)$-vs-E_B plot, (b) $\zeta_C(E_B)$-vs-E_B plot, (c) $\delta\zeta_V(E_B)$-vs-E_B plot, and (d) $\delta\zeta_C(E_B)$-vs-E_B plot calculated for the SHG coefficient d_{31} of NCSSe (**2**). The values of the functions are in pm/V. The PRF functionals are described in S1.2.

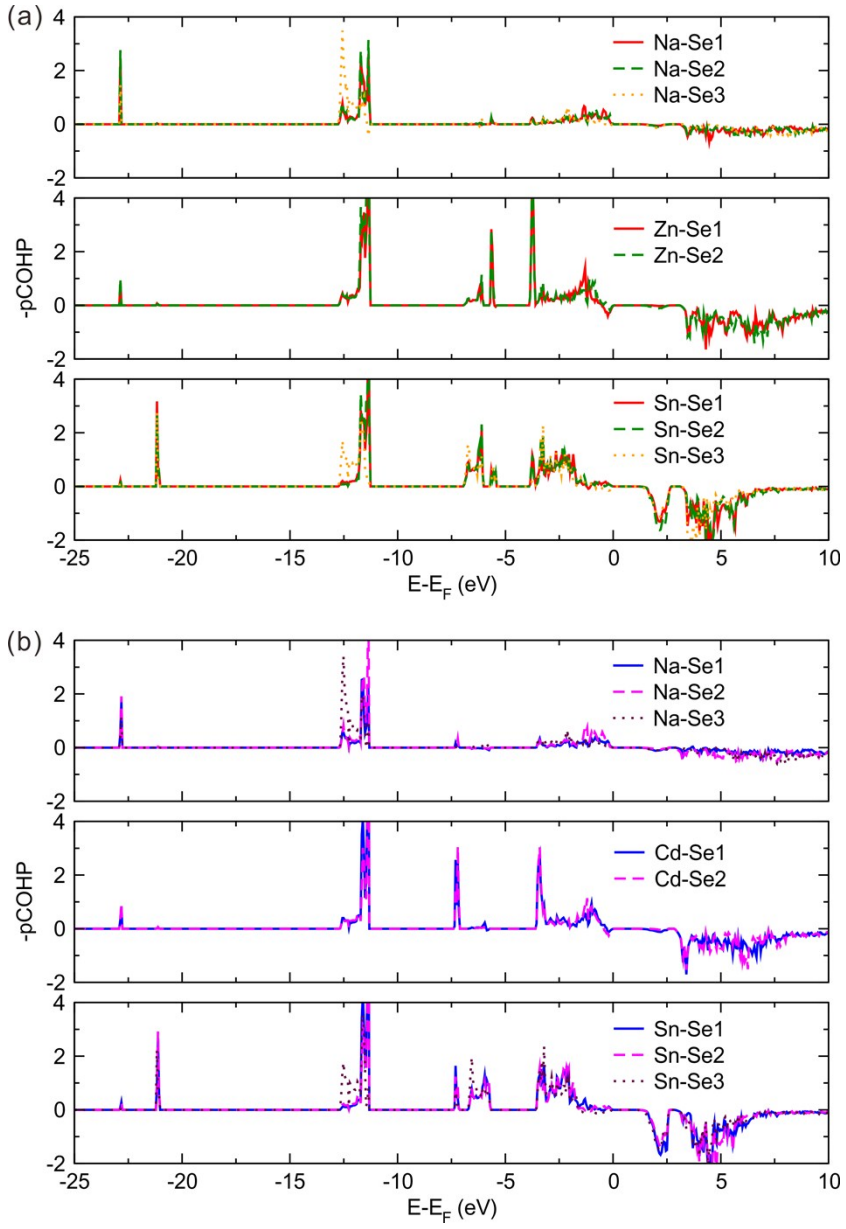

Figure S8. Projected crystal orbital Hamilton population (pCOHP) plots describing (a) the Na-Se, Zn-Se and Sn-Se bonding in **1** and (b) the Na-Se, Cd-Se and Sn-Se bonding in **2**.

References

1 (1) (a) Hohenberg, P.; Kohn, W. Inhomogeneous electron gas. *Phys. Rev.* **1964**, *136*, B864. (b) Kohn, W.; Sham, L. J. Self-consistent equations including exchange and correlation effects. *Phys. Rev. A* **1965**, *140*, 1133.

2 (2) (a) Kresse, G.; Hafner, J. *Ab initio* molecular dynamics for liquid metals. *Phys. Rev. B* **1993**, *47*, 558. (b) Kresse, G.; Furthmüller, J. Efficiency of ab-initio total energy calculations for metals and semiconductors using a plane-wave basis set. *Comput. Mat. Sci.* **1996**, *6*, 15. (c) Kresse, G.; Furthmüller, J. Efficient iterative schemes for *ab initio* total-energy calculations using a plane-wave basis set. *Phys. Rev. B* **1996**, *54*, 11169.

3 (3) Blöchl, P. E. Projector augmented-wave method. *Phys. Rev. B* **1994**, *50*, 17953.

4 (4) Perdew, J. P.; Burke, K.; Ernzerhof, M. Generalized gradient approximation made simple. *Phys. Rev. Lett.* **1996**, *77*, 3865.

5 (5) Perdew, J. P.; Wang., Y. Accurate and simple analytic representation of the electron-gas correlation energy. *Phys. Rev. B* **1992**, *45*, 13244.

6 (6) Gonze, X.; Lee, C. Dynamical matrices, Born effective charges, dielectric permittivity tensors, and interatomic force constants from density-functional perturbation theory. *Phys. Rev. B* **1997**, *55*, 10355.

7 (7) Cheng, X. Y.; Whangbo, M.-H.; Guo, G.-C.; Hong, M. C.; Deng, S. Large second harmonic generation of $LiCs_2PO_4$ caused by the metal-cation-centered groups. *Angew. Chem. Int. Ed.* **2018**, *57*, 3933. (The software for ART analysis can be obtained upon request after it is officially released.)

8 (8) (a) Aversa, C.; Sipe, J. E. Nonlinear optical susceptibilities of semiconductors: results with a length-gauge analysis. *Phys. Rev. B* **1995**, *52*, 14636. (b) Rashkeev, S. N.; Lambrecht, W. R.; Segall, B. Efficient ab initio method for the calculation of frequency-dependent second-order optical response in semiconductors. *Phys. Rev. B* **1998**, *57*, 3905. (c) Rashkeev, S. N.; Lambrecht, W. R. L. Second-harmonic generation of I-III-VI_2 chalcopyrite semiconductors: effects of chemical substitutions. *Phys. Rev. B* **2001**, *63*. (d) Sharma, S.; Dewhurst, J. K.; Ambrosch-Draxl, C. Linear and second-order optical response of III-V monolayer superlattices. *Physical Review B* **2003**, *67*. (e) Sharma, S.; Ambrosch-Draxl, C. Second-harmonic optical response from first principles. *Phys. Scripta* **2004**, *2004*, 128.

9 (9) Heyd, J.; Peralta, J. E.; Scuseria, G. E.; Martin, R. L. Energy band gaps and lattice parameters evaluated with the Heyd-Scuseria-Ernzerhof screened hybrid functional. *J. Chem. Phys.* **2005**, *123*, 174101.

10 (10) Li, G.; Wu, K.; Liu, Q.; Yang, Z.; Pan, S. $Na_2ZnSn_2S_6$: A mixed-metal thiostannate with large second-harmonic generation response activated by penta-tetrahedral $[ZnSn_4S_{14}]^{10-}$ clusters. *Sci. China Tech. Sci.* **2017**, *60*, 1465.

11 (11) Li, G.; Wu, K.; Liu, Q.; Yang, Z.; Pan, S. $Na_2ZnGe_2S_6$: A new infrared nonlinear optical material with good balance between large second-harmonic generation response and high laser damage threshold. *J. Am. Chem. Soc.* **2016**, *138*, 7422.

12 (12) Li, G. M.; Liu, Q.; Wu, K.; Yang, Z. H.; Pan, S. L. $Na_2CdGe_2Q_6$ (Q = S, Se): two metal-mixed chalcogenides with phase-matching abilities and large second-harmonic generation responses. *Dalton Trans.* **2017**, *46*, 2778.